



Theoretical study of hydrogen impact on concentration of intrinsic point defects during Czochralski Si crystal growth

Takuya Kusunoki^a, Koji Sueoka^{b,*}, Wataru Sugimura^c, Masataka Hourai^c

^a Graduate School of Engineering, Okayama Pref. Univ., Japan

^b Okayama Pref. Univ., Japan

^c SUMCO Corporation, Japan

ARTICLE INFO

Keywords:

Czochralski Si crystal growth A2
Intrinsic point defect A1
Hydrogen doping A1
Density functional theory A1
Formation energy A1

ABSTRACT

Control of intrinsic point defects (vacancy *V* and interstitial *I*) at the atomic level is required for Si substrates to satisfy the performance demands of the latest semiconductor devices. Sugimura et al. (2014) recently reported that doping hydrogen (H) atoms during Czochralski Si crystal growth affects the point defect behavior in two ways: (i) Si crystal becomes more *V* rich and (ii) the formation of dislocation clusters is suppressed. The finding of (ii) suggests that H-doping is a promising technique for the mass production of Si substrates used for power devices, among other applications. However, the effect of H-doping on point defect behavior during Si crystal growth is not yet fully understood. The purpose of the present study is to clarify the finding of (i). We performed first principles calculation of the formation energy and formation (vibration) entropy of *V* and *I* in the area influenced by the H atom in supercells composed of 64 and 216 Si atoms and then obtained the concentration of point defects incorporated at the melt/solid interface on the basis of the results. Our main findings are as follows. (1) There are three structures of hydrogen-vacancy complex (H-V) where the *V* formation energy remarkably decreases and four structures of hydrogen-interstitial Si complex (H-I) where the *I* formation energy remarkably decreases. (2) The H impact on *V* concentration is larger than that on *I* concentration and becomes apparent when H concentration is higher than $10^{15}/\text{cm}^3$. (3) The experimental finding of H impact on the concentration of intrinsic point defects is explained quantitatively.

1. Introduction

In the growth of Si single crystals using the Czochralski method, intrinsic point defects (vacancy *V* and interstitial *I*) are incorporated from the melt/solid interface at the thermal equilibrium concentration of the Si melting point. After the pair recombination of *V* and *I*, the resulting dominant *V* or *I* agglomerates to form secondary defects such as void defects or dislocation clusters. Voronkov proposed a model in which the dominant point defect is determined by the critical value v/G (v : pulling rate, G : axial thermal gradient at the melt/solid interface), and *V* becomes dominant when v/G is larger than the critical value (and vice versa) [2]. The Voronkov model is generally accepted as it accurately reproduces secondary defect distributions in grown Si crystals [3–5]. By taking the window for a defect-free Si pulling condition into consideration, defect-free Si wafers containing no measurable secondary defects are now standard in the mass production of 300-mm-diameter wafers [6,7].

The Voronkov model is affected by substitutional dopants and interstitial impurities depending on their type and concentration [8–10]. Recent density functional theory (DFT) calculations have successfully explained the experimental data of the impact of p-type (B, Ga), n-type (P, As, Sb, and Bi), and electrically neutral (C, Ge, and Sn) dopants and interstitial impurities (O) on the concentration of *V* and *I* during Si crystal growth [11–13].

Prior investigations have shown that hydrogen (H) atoms easily diffuse into Si wafers during the manufacturing process of semiconductor devices and affect the electrical properties of Si [14]. The effect of H atoms has both advantages and disadvantages for Si-based semiconductor devices. In an example of the former case, the H atom inactivates the harmful deep levels in Si bandgap caused by the impurities, defects, and so on. This is known as hydrogen passivation, and the most famous technique is to apply H termination to the dangling bonds existing at the Si and SiO_2 interface of MOS devices [14]. In the latter case, the H atom interacts with an electrically inactive impurity (e.g.,

* Corresponding author.

E-mail address: sueoka@c.oka-pu.ac.jp (K. Sueoka).

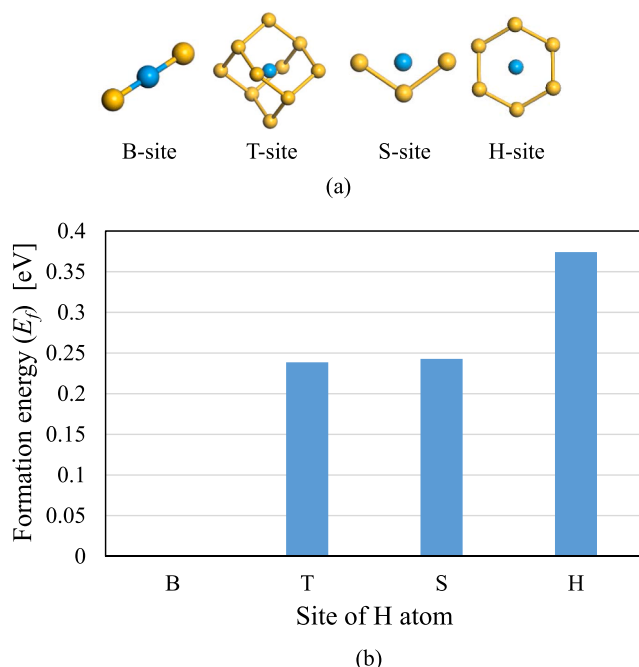


Fig. 1. (a) Atomic configuration of H atom at B-site, T-site, S-site, H-site (H: blue ball, Si: yellow ball). (b) Calculated formation energy (E_f) of H atom in Si referred to the $E_f = 1.61$ eV of H atom at B-site. Here, E_f of H atom in Si was calculated from the energy difference between H atom of H_2 molecule in vacuum slab and H atom in Si.

substitutional C) and forms electrically active complexes with harmful deep levels [15].

H atoms also interact with intrinsic point defects in Si crystals

[14,16]. When it comes to the effect of H-doping on the point defect behavior during Si crystal growth, only experimental results for Floating-Zone Si crystals have been reported [17]. Recently, Sugimura et al. reported for the first time on the experimental results of the impact of H-doping on Si crystal grown with Czochralski method [1]. They showed that the H-doping affects the point defect behavior in two ways: (i) Si crystal becomes more V rich and (ii) the formation of dislocation clusters is suppressed. The finding of (ii) suggests that H-doping is a promising technique for the mass production of Si substrates used in power devices, among other applications. However, the effect of H-doping on point defect behavior during Si crystal growth is not yet fully understood.

The purpose of the present study is to clarify the finding of (i) by means of first principles calculation of the formation energy and formation (vibration) entropy of V and I in the area influenced by the H atom in supercells composed of 64 and 216 Si atoms. A unique feature of this research is that stable configurations of hydrogen-vacancy complex (H-V) and hydrogen-interstitial Si complex (H-I) were screened without any omission by calculating the impact of H atoms on the formation energy of V and I while considering all the possible atomic configurations in a 64-Si-atom cubic cell. We were also able to obtain the more reliable data for stable complexes by using 216-Si-atom cubic cells than that obtained by using 64-Si-atom cubic cell.

The concentration of V and I incorporated at the melt/solid interface of H-doped Si crystal was calculated from the results by determining the coordination number of each V, I configuration around the H atom and using the obtained formation energy and entropy values. We then compared the theoretical results to the experimental results reported by Sugimura et al. to clarify the mechanism underlying the H impact on the point defect concentration during Si crystal growth [1,18].

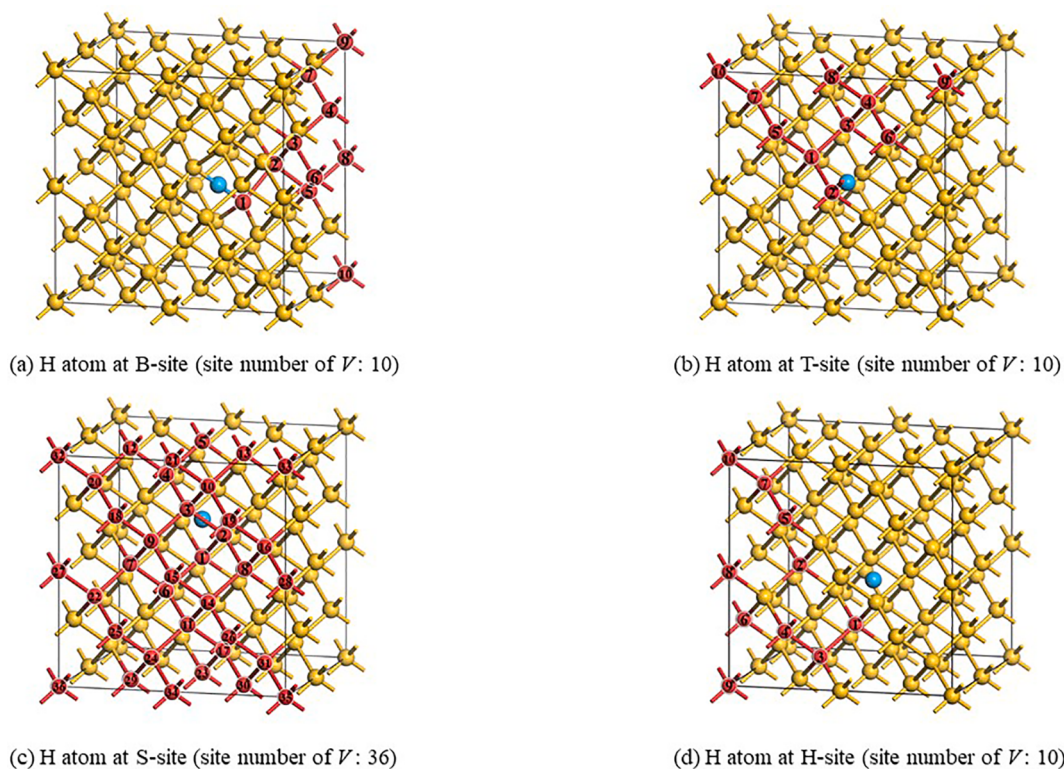


Fig. 2. All of the nearest V sites (red balls) around H atom (blue ball) in 64-Si-atom model with H atom at (a) B-site, (b) T-site, (c) S-site, and (d) H-site. The position of V is numbered in the order of distance from H atom. (For interpretation of the references to colour in this figure legend, the reader is referred to the web version of this article.)

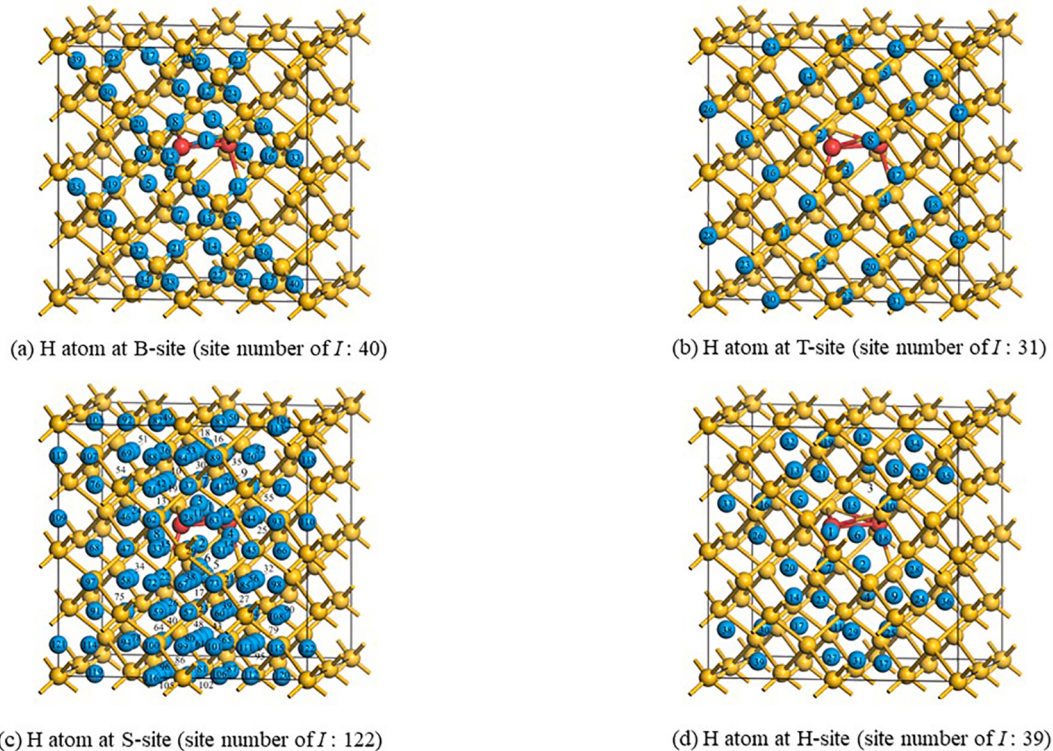


Fig. 3. All of the nearest H sites (blue balls) around I (one of the two red balls) in 64-Si-atom model with H atom at (a) B-site, (b) T-site, (c) S-site, and (d) H-site. The position of H atom is numbered in the order of distance from I . (For interpretation of the references to colour in this figure legend, the reader is referred to the web version of this article.)

2. Calculation details

We carried out the DFT calculations within the generalized gradient approximation (GGA) for electron exchange and correlation using the CASTEP code [19]. The detail procedure to optimize the electronic structure and atomic configurations can be found in Refs. [11–13]. The cut-off energy of the plane waves was 340 eV. We carried out k-point sampling at $2 \times 2 \times 2$ special points in a Monkhorst-Pack grid [20], which was sufficient to obtain converged results for the 64-Si-atom and the 216-Si-atom supercells.

Periodic boundary conditions were used with cubic supercells of 64 Si atoms and 216 Si atoms for the total energy (E_{tot}) calculation of perfect, V , I , and/or H-containing Si crystals. As a preliminary calculation, the formation energy of the H atom at typical interstitial sites was obtained. Fig. 1(a) and (b) shows the atomic configuration of the H atom (Bond center (B)-site, Tetrahedral (T)-site, Split interstitial (S)-site, and Hexagonal (H)-site) and the formation energy (E_f) after geometry optimization. The most stable site for the H atom was the B-site. The E_f at the T-site and S-site was about 0.24 eV higher, and the E_f at the H-site was about 0.36 eV higher than that at the B-site. Since the energy differences between the B-, T-, S-, and H-sites were rather small, we consider all four of these sites.

First, we performed calculations with a 64-atom supercell to screen the stable configurations of V and I around the H atom. The E_f^V of V in a perfect Si crystal is calculated by

$$E_f^V = E_{tot}[Si_{63}V_1] - E_{tot}[Si_{64}] \times \frac{63}{64}, \quad (1)$$

where $E_{tot}[Si_{64}]$ and $E_{tot}[Si_{63}V_1]$ are the total energies of a 64-Si-atom supercell and a cell including one V , respectively.

Fig. 2 shows the initial positions (before geometry optimization) of V (red balls) around the H atom (blue ball) at the B-site, T-site, S-site, and H-site while considering the crystal symmetry of Si. Note that all of the nearest positions in the model of 64 Si atoms are covered and numbered on each V site. The $E_f^{V,dope}$ of V around the H atom at the X-site (X = B, T, S, H) is calculated by

$$E_f^{V,dope} = E_{tot}[Si_{63}H_1^{X-site}V_1] - E_{tot}[Si_{64}H_1^{X-site}] + E_{tot}[Si_{64}] \times \frac{1}{64}, \quad (2)$$

where $E_{tot}[Si_{63}H_1^{X-site}V_1]$ and $E_{tot}[Si_{64}H_1^{X-site}]$ are the total energies of a 64-Si-atom cell including one V and one H atom at the X-site and a cell including one H atom at the X-site, respectively.

It is known that I is most stable at the [110] dumbbell (D)-site in a perfect Si crystal [13]. The E_f^I of I in a perfect Si crystal is calculated by

$$E_f^I = E_{tot}[Si_{64}I_1] - E_{tot}[Si_{64}] \times \frac{65}{64}, \quad (3)$$

where $E_{tot}[Si_{64}]$ and $E_{tot}[Si_{64}I_1]$ are the total energies of a 64-Si-atom supercell and a cell including one I , respectively.

We examined the initial positions of I around the H atom by placing I at the center of the mode and then changing the relative location of the H atom around I . Fig. 3 shows the initial positions of the H atom (blue) at the B-site, T-site, S-site, and H-site around I (one of two red balls) while considering the crystal symmetry of Si. Note that all of the nearest positions of the H atom around I (this is the same as the nearest positions of

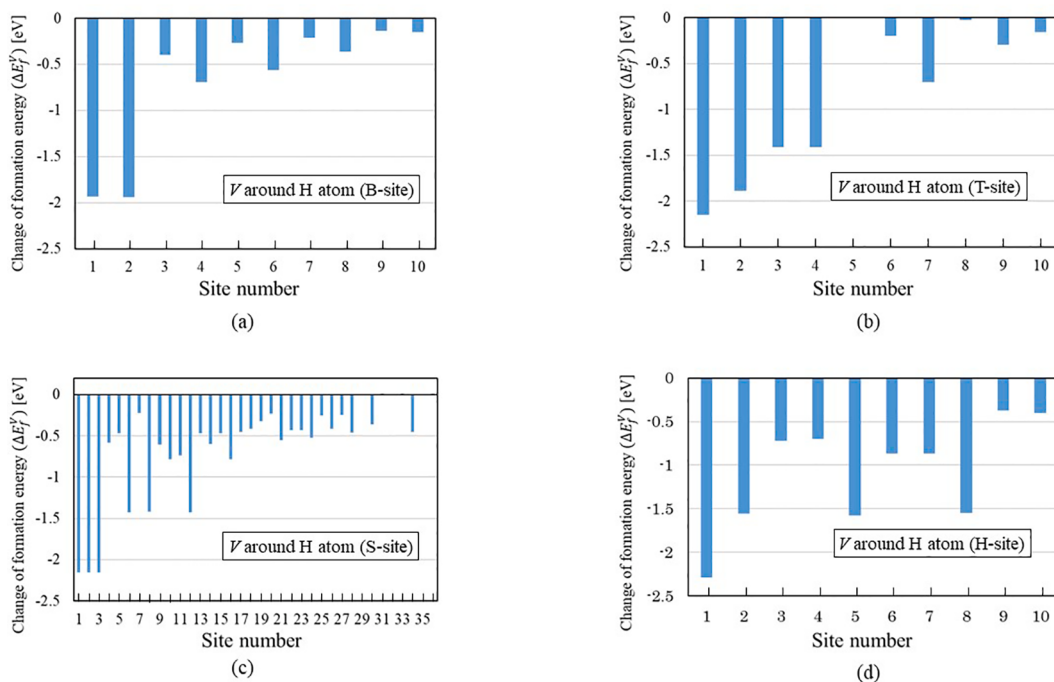


Fig. 4. Calculated change of E_f of V ($\Delta E_f^V = E_f^{V,dope} - E_f^V$) due to the effect of H atom in the 64-Si-atom model. H atom is located at (a) B-site, (b) T-site, (c) S-site, and (d) H-site.

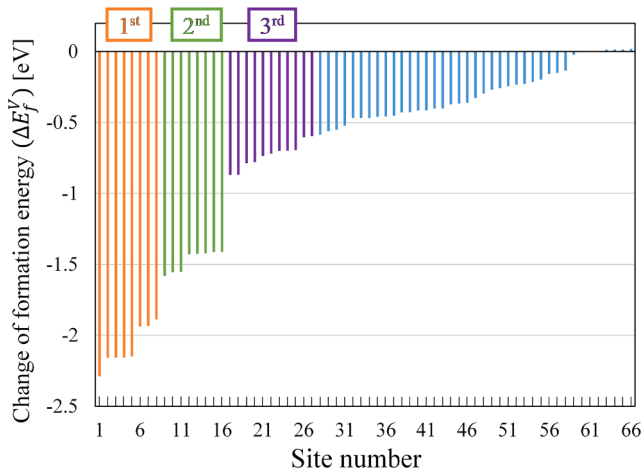


Fig. 5. All data of ΔE_f^V of V around H atom at B-site, T-site, S-site, and H-site sorted in ascending order. ΔE_f^V of three energetically favorable atomic structures are shown as 1st (orange), 2nd (green), and 3rd (purple). (For interpretation of the references to colour in this figure legend, the reader is referred to the web version of this article.)

I around the H atom) in the model of 64 Si atoms are covered and numbered on each H atom site. The $E_f^{I,dope}$ of I around the H atom at the X-site (X = B, T, S, H) is calculated by

$$E_f^{I,dope} = E_{tot}[Si_{64}H_1^{X-site}I_1] - E_{tot}[Si_{64}H_1^{X-site}] - E_{tot}[Si_{64}] \times \frac{1}{64}, \quad (4)$$

where $E_{tot}[Si_{64}H_1^{X-site}I_1]$ and $E_{tot}[Si_{64}H_1^{X-site}]$ are the total energies of a 64-Si-atom cell including one I and one H atom at the X-site and a cell including one H atom at the X-site, respectively.

After screening the stable configurations of V or I around the H atom by using the 64-atom supercell, we performed calculations with a 216-atom model including V and I at the center to obtain a more reliable E_f of V and I . The formation (vibration) entropies (S_f) of free V (I) and V

Table 1

Calculated formation energy and formation entropies of free V and I . k_B is the Boltzmann constant.

Point defects	$E_f^{V,I}$ [eV] (Si 64 model)	$E_f^{V,I}$ [eV] (Si 216 model)	$\frac{S_f^{V,I}}{k_B}$
V	3.54 (Cal.)	3.62 (Cal.)	5.258 (Cal.)
	3.94 (Exp. [3])	8.949 (Exp. [3])	5.967 (Cal.)
	3.51 (Cal.)	3.45 (Cal.)	7.620 (Exp. [3])
I	4.05 (Exp. [3])	4.05 (Exp. [3])	7.620 (Exp. [3])

(I) around the H atom were calculated using a 64-atom supercell with the linear response method [21].

Finally, the concentration of point defects incorporated at the melt/solid interface was calculated from the results. The impact of H-doping on point defect concentrations was then compared to the reported experimental results [1,18].

Table 2

Calculated formation energy and formation entropies of V and I around H atoms.

Dopant	Point defects	$\Delta E_f^{V,I}$ [eV] (Si 64 model)	$\Delta E_f^{V,I}$ [eV] (Si 216 model)	$\frac{\Delta S_f^{V,I}}{k_B}$	Coordination number (Z_i)
H	V 1 st	-2.28 to -1.89	-2.36	-4.149	4
	V 2 nd	-1.58 to -1.41	-1.66	-18.219	4
	V 3 nd	-0.86 to -0.60	-0.87	0.123	12
	I 1 st (a)	-1.73 to -1.35	-1.62	-2.345	2
	I 1 st (b)	-1.73 to -1.60	-1.72	-2.637	4
	I 2 nd (a)	-1.30 to -1.02	-1.22	-0.760	2
	I 2 nd (b)	-1.19 to -1.08	-1.24	-1.545	4

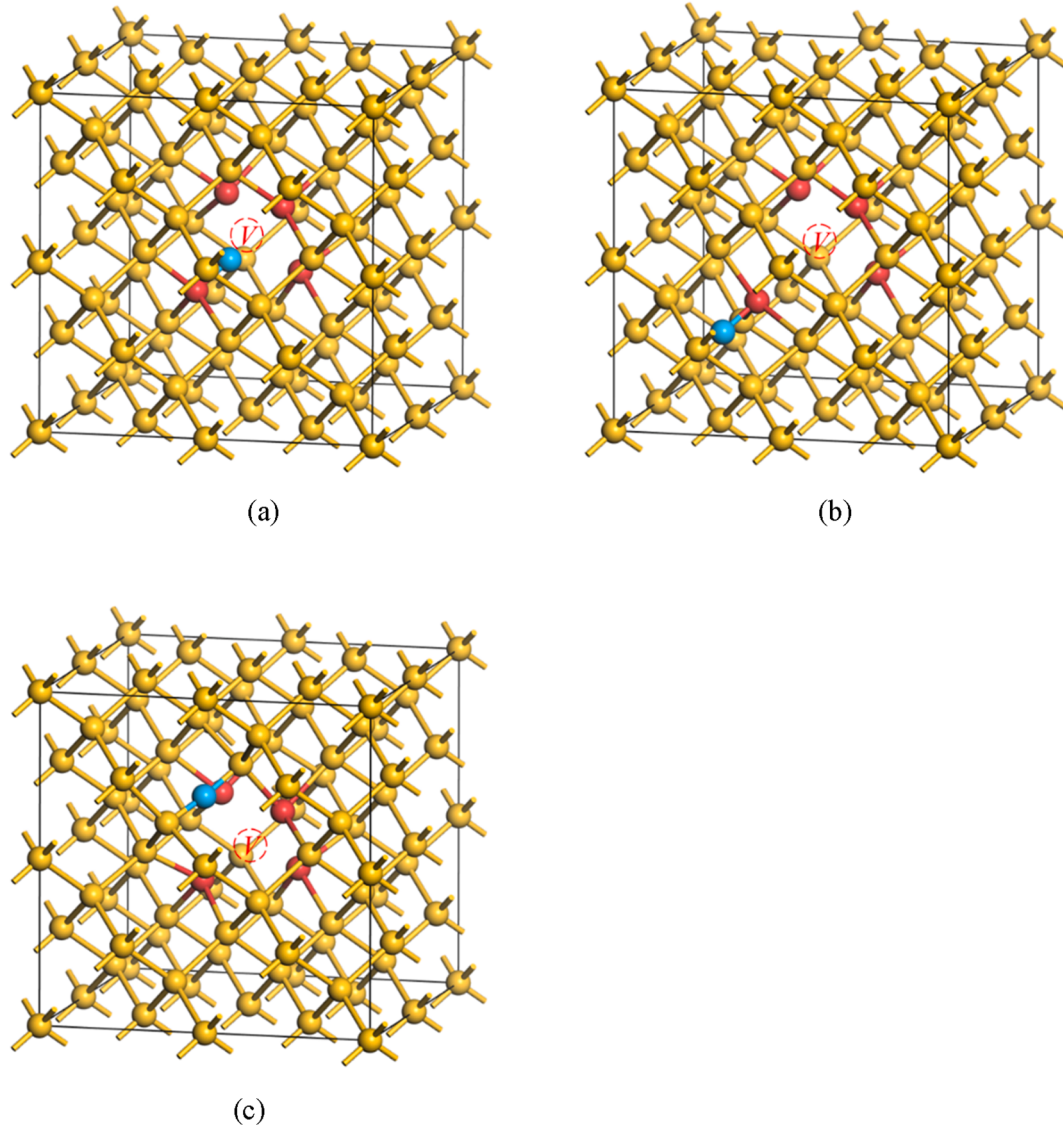


Fig. 6. (a) 1st stable structure, (b) 2nd stable structure, and (c) 3rd stable structure of V and H atom after geometry optimization. H atom is in blue and first neighboring Si atoms from V are in red. (For interpretation of the references to colour in this figure legend, the reader is referred to the web version of this article.)

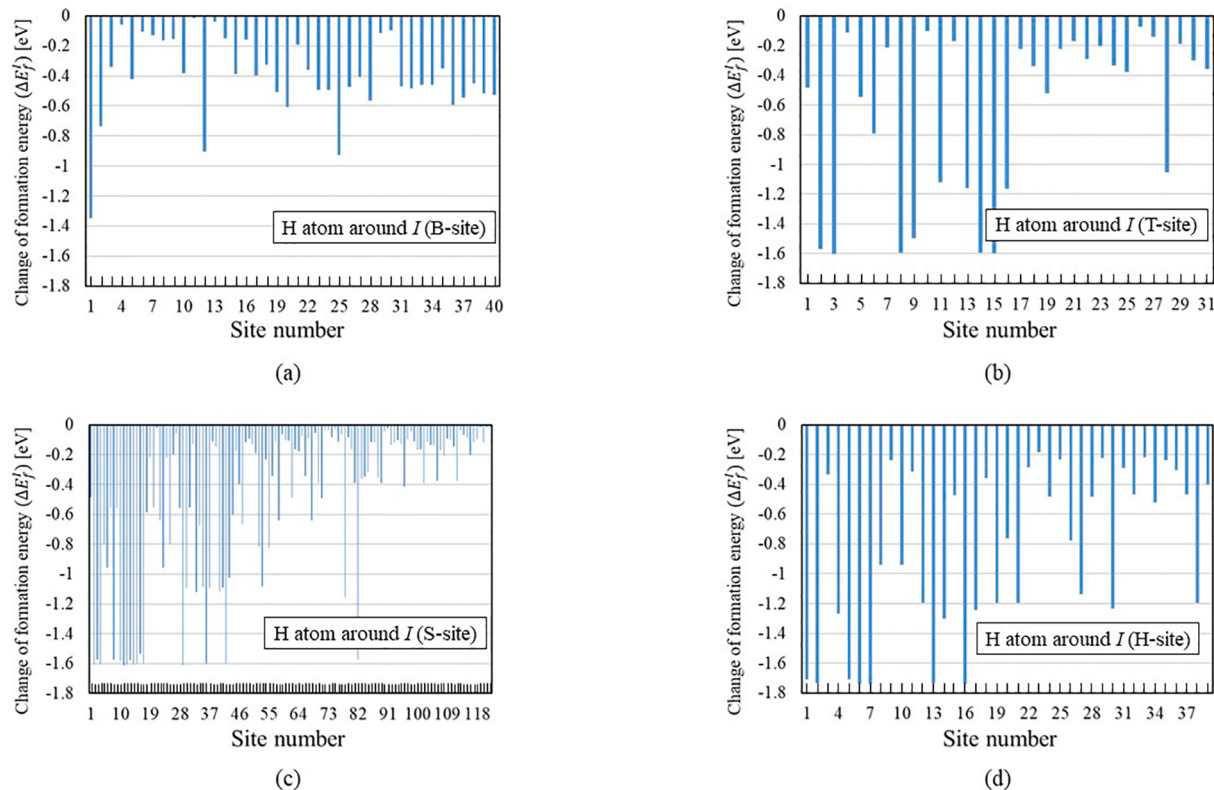


Fig. 7. Calculated change of E_f of I ($\Delta E_f^I = E_f^{I,\text{dope}} - E_f^I$) due to the effect of H atom in the 64-Si-atom model. H atom is located at (a) B-site, (b) T-site, (c) S-site, and (d) H-site.

3. Results and discussion

3.1. E_f and S_f of V (I) around H atom

3.1.1. Vacancy V

Fig. 4 shows the calculated change of the E_f of V ($\Delta E_f^V = E_f^{V,\text{dope}} - E_f^V$) due to the effect of the H atom in the 64-Si-atom model. The horizontal axis indicates the site number of V from the H atom at each site. We found that the E_f of V decreased around H atoms. Furthermore, the E_f of V depended on the site of the H atom and did not simply increase with an increase in the distance from the H atom.

Fig. 5 shows all data of the ΔE_f^V of V around the H atom at the B-site, T-site, S-site, and H-site sorted in ascending order. We confirmed that the interaction of V with the H atom did not reach beyond the 64-Si-atom model. Three energetically favorable atomic configurations appeared after the geometry optimization, which are shown as 1st, 2nd, and 3rd stable structures. In each structure, the obtained ΔE_f^V was distributed about 0.4 eV at the highest depending on the initial configurations in the 64-Si-atom cell. This is due to the limited cell size (interaction with image cells), and a more reliable ΔE_f^V was obtained by using a 216-atom supercell. The calculated E_f and S_f of V in perfect Si and V for the 1st, 2nd, and 3rd stable structures around the H atom are summarized in Tables 1 and 2, respectively.

Fig. 6(a) shows the 1st stable structure of V and H atom after geometry optimization. The H atom terminated one of the four dangling bonds of V . The 2nd stable structure of V and H atom is shown in (b). The H atom bonded in the [1 1 1] direction of the first neighboring Si atom from V . The 3rd stable structure of V and H atom is shown in (c). The H atom stayed at the B-site between the second and third neighboring Si atoms from V .

The other V sites from the H atom in Fig. 5 had relatively larger energies than those of the 1st, 2nd, and 3rd stable structures. A rough estimation using Eq. (5) in Sec. 3.2 showed that the impact of V at the other sites was less than 0.3% of the total concentration of V . Therefore, we considered only the 1st, 2nd, and 3rd structures for the calculation of V concentration in Section 3.2.

3.1.2. Self-Interstitial I

Fig. 7 shows the calculated change of the E_f of I ($\Delta E_f^I = E_f^{I,\text{dope}} - E_f^I$) due to the effect of the H atom in the Si-64-atom model. The horizontal axis indicates the site number of I from H at each site. We found that the E_f of I also decreased around H atoms. Furthermore, the E_f of I depended on the site of the H atom and did not simply increase with an increase in the distance from the H atom.

Fig. 8 shows all data of the ΔE_f^I of I around the H atom at the B-site, T-site, S-site, and H-site sorted in ascending order. We confirmed that the

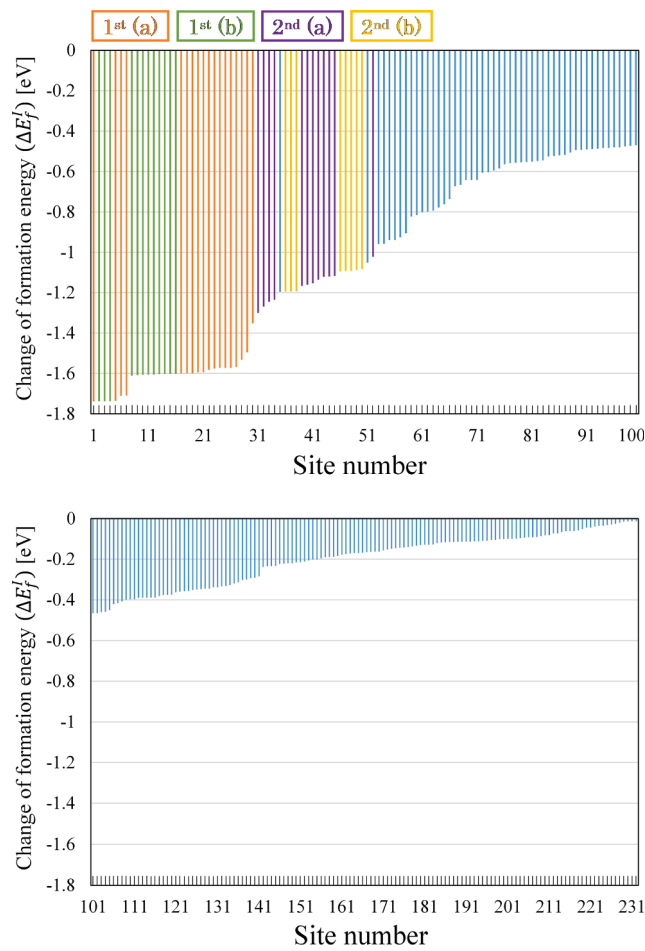


Fig. 8. All data of ΔE_f^I of I around H atom at B-site, T-site, S-site, and H-site sorted in ascending order from 1 to 100 (upper) and more than 100 (below). ΔE_f^I of four energetically favorable atomic structures are shown as 1st(a) (orange), 1st(b) (green), 2nd(a) (purple), and 2nd(b) (yellow). (For interpretation of the references to colour in this figure legend, the reader is referred to the web version of this article.)

interaction of I with the H atom does not reach beyond the 64-Si-atom model. Four energetically favorable atomic structures appeared after the geometry optimization, which are shown as 1st(a) stable structure, 1st(b) stable structure, 2nd(a) stable structure, and 2nd(b) stable structure. The E_f of structures 1st(a) and 1st(b) were the lowest and almost the same as each other. The E_f of structures 2nd(a) and 2nd(b) were the 2nd lowest and almost the same as each other. In each structure, the obtained E_f was distributed about 0.4 eV at the highest depending on the initial configurations. This is due to the same reason as the V case, and a more reliable E_f was obtained by using a 216-atom supercell. The calculated E_f and S_f of I in perfect Si and I for the 1st and 2nd stable structures around the H atom are summarized in Tables 1 and 2, respectively.

Fig. 9(a) shows one of the two most stable structures of I and H atom (structure 1st(a)) after geometry optimization. The H atom bonded to one of I at the D-site along the [1 1 0] direction. The other most stable structure (1st(b)) is shown in (b). The H atom bonded to one of I at the D-site along the [1 1 1] direction. One of the second-most stable structures of I and H atom (structure 2nd(a)) is shown in (c). The H atom bonded to the Si atom that was apart from I at the D-site. The other second-most stable structure (2nd(b)) is shown in (d). The H atom bonded to the Si atom that was apart from I at the D-site.

The other I in Fig. 8 had relatively larger energies than those in structures 1 and 2. A rough estimation using Eq. (5) in Section 3.2 showed that the impact of I at the other sites was less than 15.3% of the total concentration of I . Furthermore, as mentioned in the next section, the impact of H-doping on I concentration was rather small compared to that on V concentration. Therefore, we considered only the 1st and 2nd structures for the calculation of I concentration in Section 3.2.

3.1.3. Electric charges of H, Si atoms around V, and I

In this section, we discuss the mechanism of the impact of H-doping on the decrease of E_f of V and I in Si. Fig. 10(a) shows the electric charges of isolated H atom and Si atoms around it calculated using the Mulliken method [22]. Fig. 10(b) and (c) show the electric charges of Si atoms around isolated V and isolated I , respectively. The H atom is charged negatively while Si atoms around V are slightly negatively charged and I is electrically neutral.

Fig. 11(a) shows the electric charges of 1st, 2nd, and 3rd stable structures of V and H atom. In the 1st and 2nd stable structures, the Coulomb attractive force between negatively charged H atom and positively charged Si atom to which H atom is bonded is the cause of the decrease of V formation energy. In the 3rd stable structure, not an electric effect but the relaxation of strain around V by the interstitial H probably brings a decrease of V formation energy. Fig. 11(b) shows the electric charges of 1st(a), 1st(b), 2nd(a), and 2nd(b) stable structures of I and H atom. In the 1st(a) and 1st(b) stable structures, the Coulomb attractive force between negatively charged H atom and positively charged I atom to which H atom is bonded is the cause of the decrease of I formation energy. In the 2nd(a) and 2nd(b) stable structures, not an electric effect but the relaxation of strain around I by the interstitial H probably brings a decrease of I formation energy.

In the case of V (I) exists far enough away from H atom in 64-Si-atom supercell, the electric charges of V (I) and H atom did not change from the values when isolated. This result supports our confirmation that the interaction of V (I) with the H atom does not reach beyond the 64-Si-atom model.

3.2. Hydrogen impact on concentration of V and I during Si crystal growth

In this section, we evaluate the thermal equilibrium concentrations of free and trapped point defects as a function of the concentrations of H atom in Si crystal. We define the “total V or I ($C_{V,I}^{eq,tot}$)” as the sum of free V or I ($C_{V,I}^{eq,free}$) and V or I trapped by the H atoms ($C_{V,I}^{eq,trapped}$). The thermal equilibrium concentrations of trapped V and I will change due to

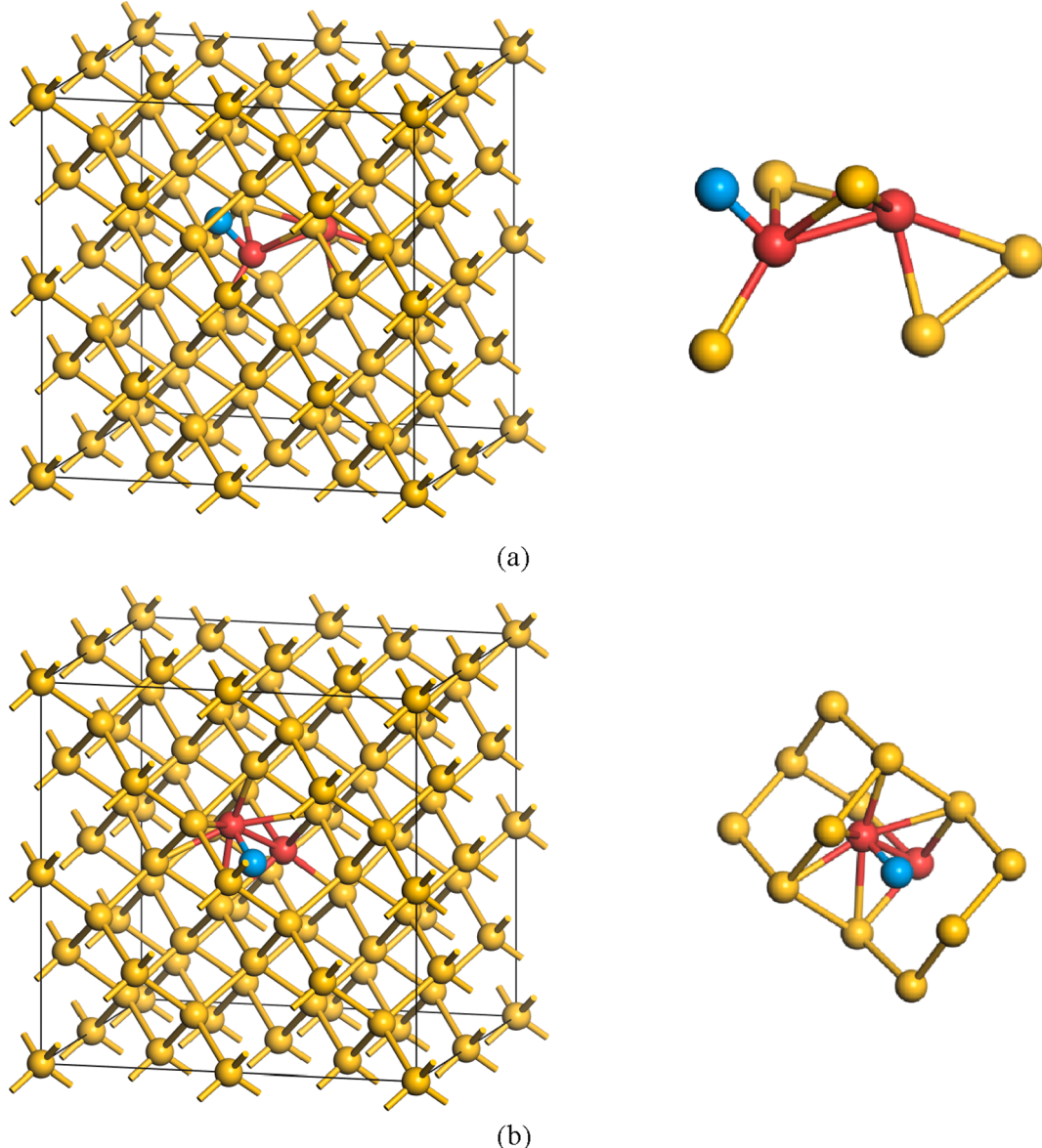


Fig. 9. (a) 1st(a) stable structure, (b) 1st(b) stable structure, (c) 2nd(a) stable structure, and (d) 2nd(b) stable structure of I and H atom after geometry optimization. H atom is in blue and Si atoms originally formed at I at D-site are in red.

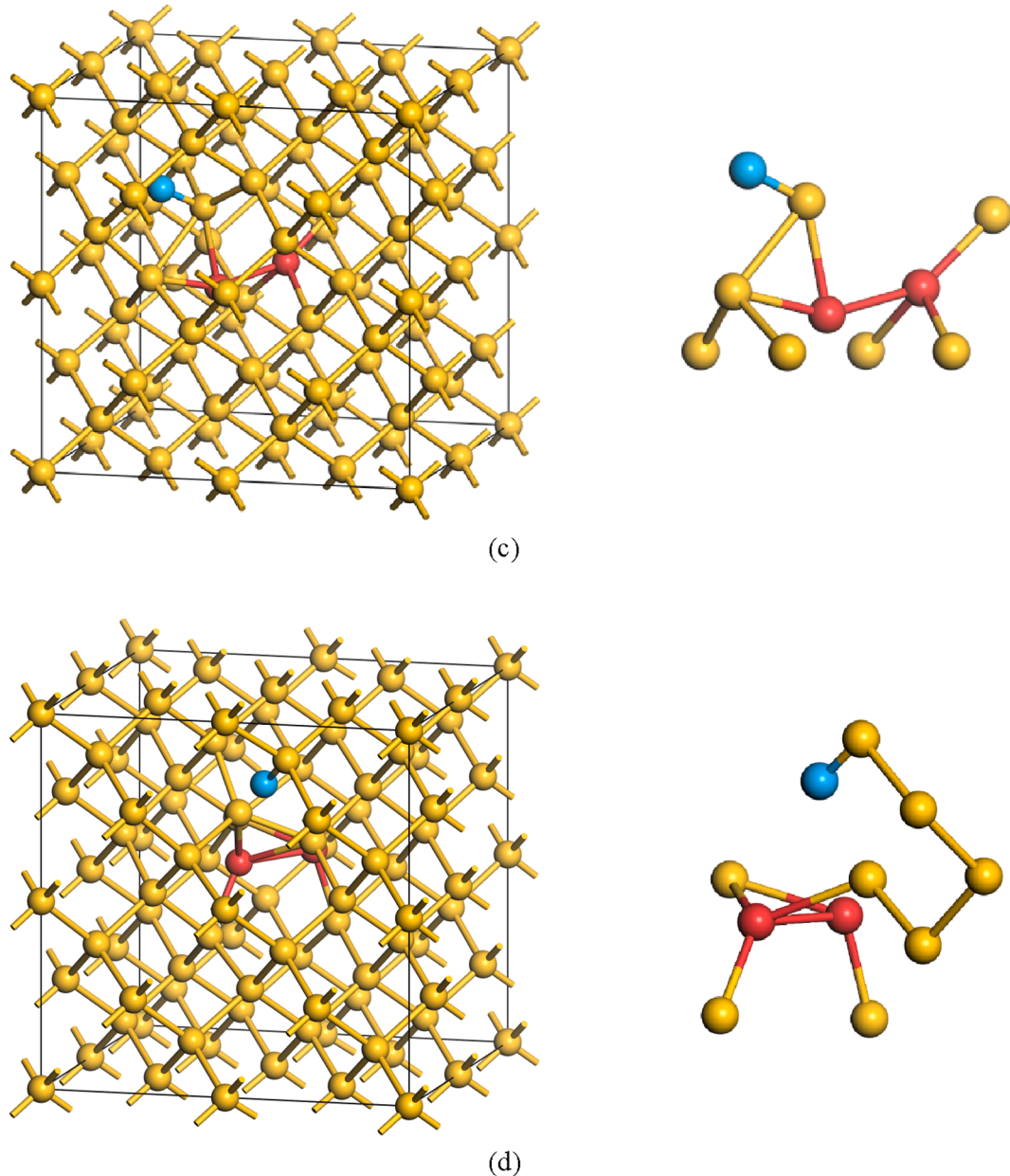


Fig. 9. (continued).

changes in the formation energies and formation entropies of the intrinsic point defects around H atoms, depending on the concentration of H atoms. The total equilibrium V and I concentrations can be written as

$$C_{V,I}^{eq,tot} = C_{V,I}^{eq,free} + C_{V,I}^{eq,trapped}$$

$$= C_{V,I,site} \left[1 - \left(\sum_{i=1}^{\frac{3}{4}(I)} Z_i \right) \frac{C_H}{C_{Si}} \right] \exp\left(\frac{S_f^{V,I}}{k_B}\right) \exp\left(-\frac{E_f^{V,I}}{k_B T_m}\right) + C_H \sum_{i=1}^{\frac{3}{4}(V)} Z_i \exp\left(\frac{S_f^{V_i,I_i(dope)}}{k_B}\right) \exp\left(-\frac{E_f^{V_i,I_i(dope)}}{k_B T_m}\right)$$

$$= \exp\left(\frac{S_f^{V,I}}{k_B}\right) \exp\left(-\frac{E_f^{V,I}}{k_B T_m}\right) \left\{ C_{V,I,site} \left[1 - \left(\sum_{i=1}^{3(V)} Z_i \right) \frac{C_H}{C_{Si}} \right] + C_H \sum_{i=1}^{4(I)} Z_i \exp\left(\frac{\Delta S_f^{V_i,I_i}}{k_B}\right) \exp\left(-\frac{\Delta E_f^{V_i,I_i}}{k_B T_m}\right) \right\}, \quad (5)$$

where $C_{V,site} = 5 \times 10^{22} \text{ cm}^{-3}$ is the number of possible V sites per unit volume, which equals the number of Si atoms per unit volume, and $C_{Si}, C_{I,site} = 3 \times 10^{23} \text{ cm}^{-3}$ is the number of I at D-sites per unit volume. The notation C_H is the H concentration. $S_f^{V,I}$ and $E_f^{V,I}$ are the formation entropy and formation energy of V and I for intrinsic Si, respectively, k_B is the Boltzmann constant, T_m is the melting point temperature, and Z_i is the coordination number at the i th site around the H atom. $\Delta E_f^{V_i,I_i} (= E_f^{V_i,I_i(\text{dope})} - E_f^{V,I})$ in the second row of Eq. (5) is the change in the formation energy of V and I at the i th site around the H atom compared to the intrinsic value. $\Delta S_f^{V_i,I_i} (= S_f^{V_i,I_i(\text{dope})} - S_f^{V,I})$ in the second row of Eq. (5) is the change in the formation entropy of V and I at the i th site around the H atom compared to the intrinsic value.

In this study, we used $S_f^{V,I}$ and $E_f^{V,I}$ values of V and I for intrinsic Si (proposed by Nakamura et al.; see Table 1), as these values can accurately reproduce actual defect distributions in the growing Si crystal [3].

$\Delta E_f^{V_i,I_i}$ and $\Delta S_f^{V_i,I_i}$ correspond to the change of formation energy and the change of formation entropy, respectively, of V and I at the i th site from the H atom. The obtained $\Delta E_f^{V_i,I_i}$, $\Delta S_f^{V_i,I_i}$, and the coordination number Z_i are summarized in Table 2 and used in the present calculation.

The H concentration dependence of the thermal equilibrium concentration of V ($C_V^{eq,tot}$) and the thermal equilibrium concentration of I ($C_I^{eq,tot}$) at the melting point was obtained. Furthermore, considering that the pair recombination of V and I occurs just below the melting point, the result of calculating $C_V^{eq,tot} - C_I^{eq,tot}$ is shown in Fig. 12. From these results, we can see that the H impact on V concentration was larger than that on I concentration and became apparent when the H concentration was higher than $10^{15}/\text{cm}^3$. We assume that the H-doping changes $C_{V,I}^{eq,tot}$ at T_m and that $C_V^{eq,tot} - C_I^{eq,tot}$ is directly proportional to the H concentration, as

$$(C_V^{eq,tot} - C_I^{eq,tot})_H = (C_V^{eq,tot} - C_I^{eq,tot})_{int} + aC_H. \quad (6)$$

Table 3 shows the results derived from the calculation of the coefficient a of H concentration and compared with the experimentally determined value [1,18]. Since the ratio (1.41) of the calculated value to

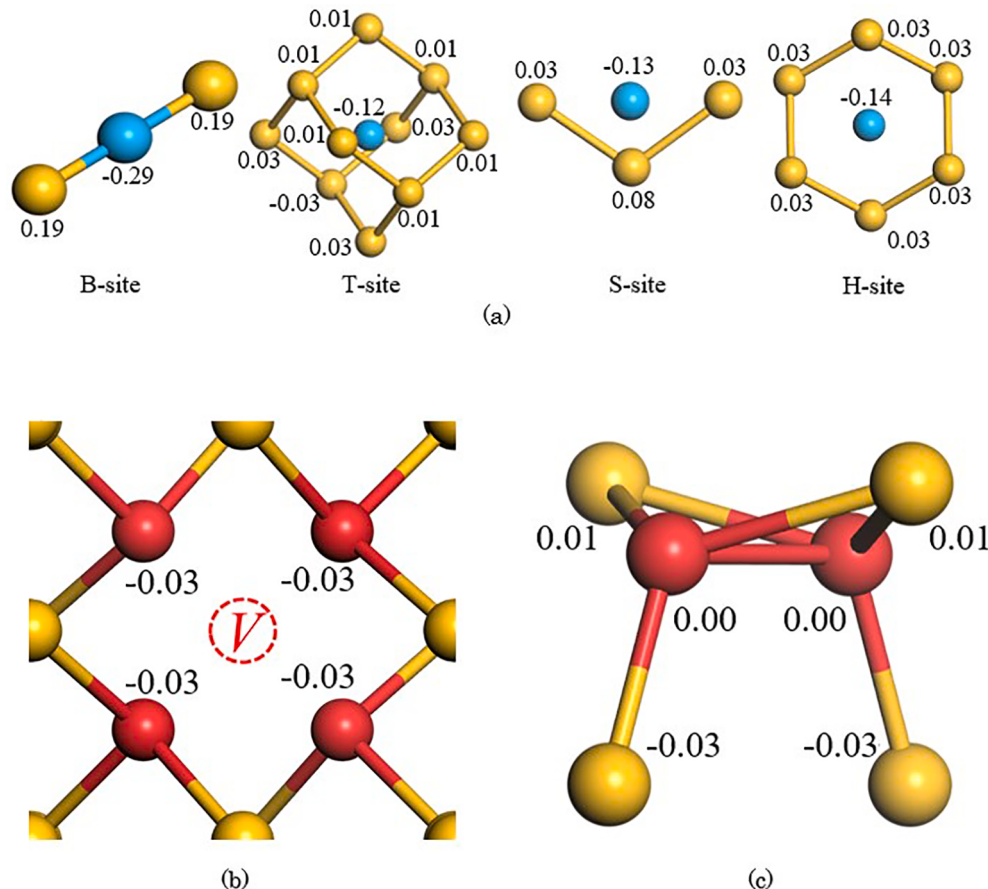


Fig. 10. Calculated electric charges of (a) isolated H atom and Si atoms around it, (b) Si atoms around isolated V, and (c) isolated I.

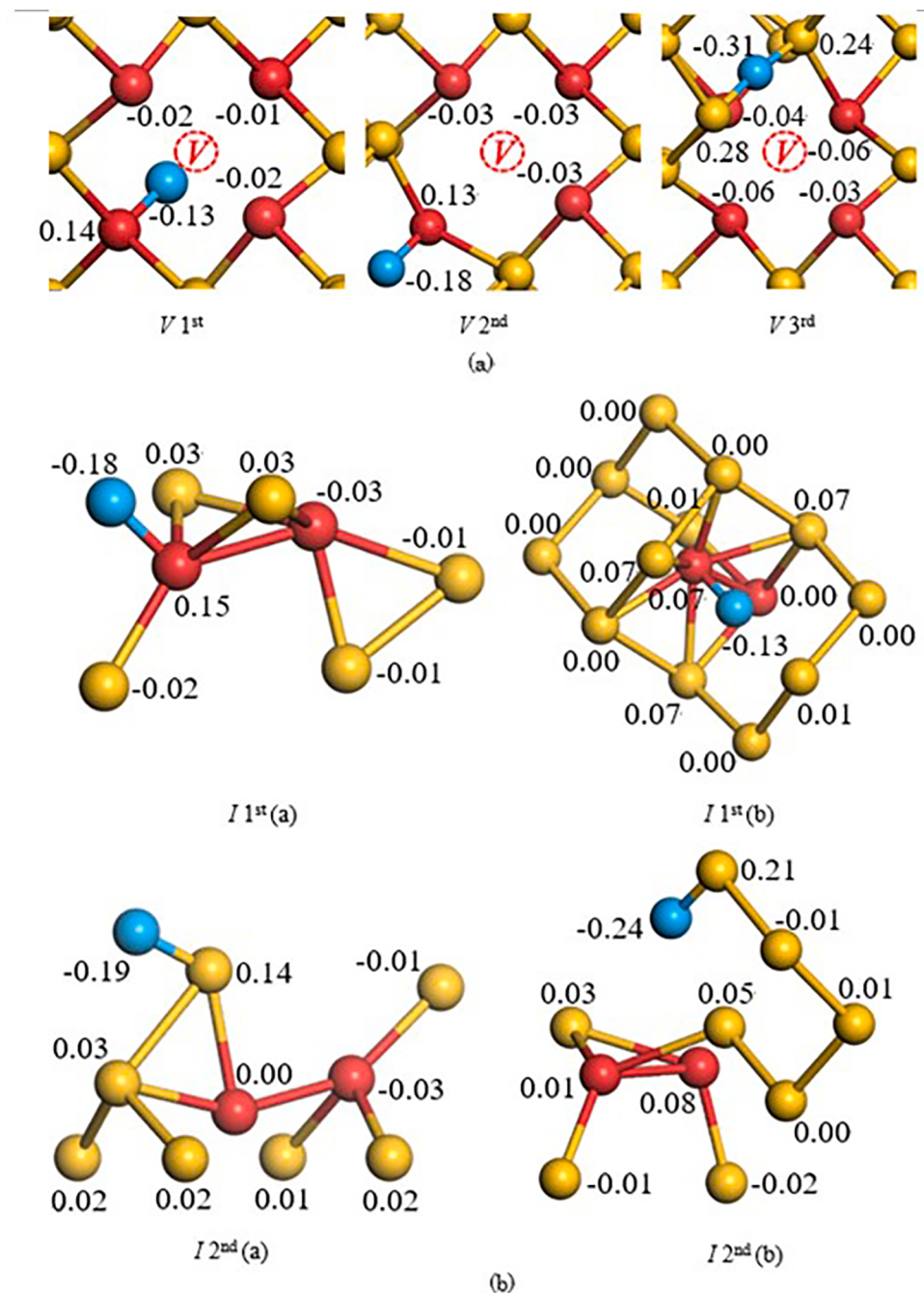


Fig. 11. Calculated electric charges of (a) 1st, 2nd, and 3rd stable structures of V and H atom, and (b) 1st(a), 1st(b), 2nd(a), and 2nd(b) stable structures of I and H atom.

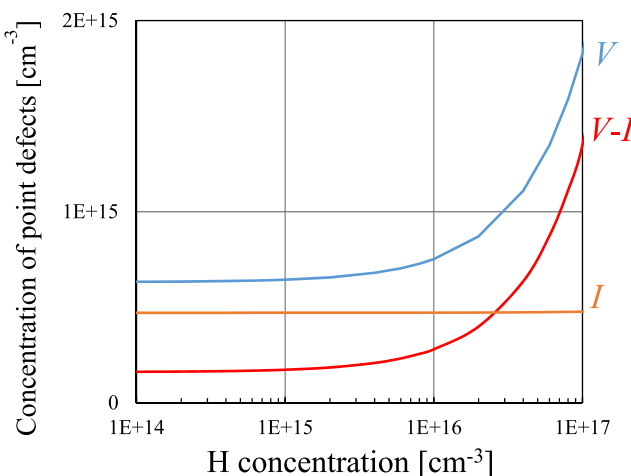


Fig. 12. Calculated dependence of V , I , and $V-I$ concentrations on the H concentration at Si melting temperature.

Table 3

Comparison of coefficient a of H concentration between experiment [1,18] and calculation.

Experiment	Calculation	Cal./Exp.
8.42×10^{-3}	1.19×10^{-2}	1.41

the experimental value is close to one, we conclude that the experimental finding of H impact on the concentration of intrinsic point defects is explained quantitatively in the present study.

4. Conclusion

We have theoretically investigated the impact of H-doping on the concentration of intrinsic point defects during Czochralski Si crystal growth. DFT calculations were performed to obtain the formation energy and formation entropy of V and I in the area influenced by H atoms in supercells composed of 64 and 216 Si atoms. A unique feature of this research is that the stable H-V and H-I configurations were screened without any omission by calculating the impact of the H atom on the formation energy of V and I while considering all the possible atomic configurations in a 64-Si-atom cubic cell. We also found that the more reliable data for stable complexes was obtained by using 216-Si-atom cubic cells.

The thermal equilibrium concentrations of trapped and total intrinsic point defects (sum of free V or I and V or I trapped with H atoms) in H-doped Si were obtained by means of DFT calculations. We found that the H impact on V concentration was larger than that on I concentration and became apparent when the H concentration was higher than $10^{15}/\text{cm}^3$. We were also able to quantitatively explain the experimental results of point defect concentration in H-doped Czochralski Si crystal reported by Sugimura et al. [1,18].

Declaration of Competing Interest

None.

Acknowledgement

This work was partially supported by a JSPS KAKENHI grant, Number 19K05294.

References

- [1] W. Sugimura, T. Ono, K. Nakamura, M. Hourai, K. Higashida, Proc. Forum Sci. Technol. Silicon Mater. 2014 (2014) 248.
- [2] V.V. Voronkov, J. Cryst. Growth 59 (1982) 625.
- [3] K. Nakamura, T. Saishoji, J. Tomioka, ECS Proc. PV 2002-2 (2002) 554.
- [4] T. Sanno, J. Cryst. Growth 303 (2007) 5.
- [5] M. Kulkarni, ECS Trans. 2 (2006) 213.
- [6] M. Hourai, E. Kajita, T. Nagashima, H. Fujiwara, S. Ueno, S. Sadamitsu, S. Miki, T. Shigematsu, Mater. Sci. Forum 196–201 (1995) 1713.
- [7] M. Hourai, H. Nishikawa, T. Tanaka, S. Umeno, E. Asayama, T. Nomachi, G. Kelly, ECS Proc. PV98-1 (1998) 453.
- [8] E. Dornberger, D. Gräf, M. Suhren, U. Lambert, P. Wagner, F. Dupret, W. Ammon, J. Cryst. Growth 180 (1997) 343.
- [9] K. Nakamura, R. Suewaka, T. Saishoji, J. Tomioka, Proc. Forum Sci. Technol. Silicon Mater. 2003 (2003) 161 (and references therein).
- [10] T. Abe, J. Cryst. Growth 334 (2011) 4.
- [11] K. Sueoka, E. Kamiyama, J. Vanhellemont, J. Appl. Phys. 114 (2013), 153510 (and references therein).
- [12] K. Sueoka, K. Nakamura, J. Vanhellemont, J. Cryst. Growth 474 (2017) 89.
- [13] K. Sueoka, Y. Mukaiyama, S. Maeda, M. Iizuka, V. Mamedov, ECS, J. Solid State Sci. and Tech. 8 (2019) P228 (and references therein).
- [14] S. Streicher, M. Stavola, J. Weber, Silicon, Germanium, and Their Alloys, CRC Press (2015) 217 (and references therein).
- [15] J.W. Lyding, K. Hess, I.C. Kizilyalli, Appl. Phys. Lett. 68 (1996) 2526.
- [16] M. Suezawa, J. Appl. Phys. 83 (1998) 1958.
- [17] T.H. Wang, J. Cryst. Growth 109 (1991) 155.
- [18] K. Nakamura, Proceedings of the Forum on the Science and Technology of Silicon Materials 2018 (2018) 1 (and references therein).
- [19] The CASTEP code is available from Dassault Systems Biovia Inc.
- [20] H. Monkhorst, J. Pack, Phys. Rev. B 13 (1976) 5188.
- [21] S. Baroni, S. de Gironcoli, A. Dal Corso, P. Giannozzi, Rev. Mod. Phys. 73 (2001) 515.
- [22] R.S. Mulliken, J. Chem. Phys. 23 (1955) 1833.